New Journal of Physics
The open-access journal for physics

Unconventional spin texture of a topologically nontrivial semimetal Sb(110)

A Strożecka[1], A Eiguren[2,3], M Bianchi[4], D Guan[4], C H Voetmann[4], S Bao[5], Ph Hofmann[4] and J I Pascual[1,6,7,8]

[1] Institut für Experimentalphysik, Freie Universität Berlin, D-14195 Berlin, Germany
[2] Departameto de Física de la Materia Condensada, UPV/EHU, Barrio Sarriena s/n, E-48940 Leioa, Spain
[3] Donostia International Physics Center (DIPC), Paseo Manuel de Lardizabal, 4, E-20018 Donostia-San Sebastian, Spain
[4] Department of Physics and Astronomy, Interdisciplinary Nanoscience Center, Aarhus University, DK-8000 Aarhus C, Denmark
[5] Department of Physics, Zhejiang University, Hangzhou 310027, China
[6] IKERBASQUE, Basque Foundation for Science, 48011 Bilbao, Spain
[7] CIC nanoGUNE, 20018 Donostia-San Sebastián, Spain
E-mail: ji.pascual@nanogune.eu

New Journal of Physics **14** (2012) 103026 (9pp)
Received 8 June 2012
Published 17 October 2012
Online at http://www.njp.org/
doi:10.1088/1367-2630/14/10/103026

Abstract. The surfaces of antimony are characterized by the presence of spin-split states within the projected bulk band gap and the Fermi contour is thus expected to exhibit a spin texture. Using spin-resolved density functional theory calculations, we determine the spin polarization of the surface bands of Sb(110). The existence of the unconventional spin texture is corroborated by the investigations of the electron scattering on this surface. The charge interference patterns formed around single scattering impurities, imaged by scanning tunneling microscopy, reveal the absence of direct backscattering signal. We identify the allowed scattering vectors and analyze their bias evolution in relation to the surface-state dispersion.

[8] Author to whom any correspondence should be addressed.

Pure bismuth and antimony are group-V semimetals and their surfaces support spin–orbit split surface states existing within the projected bulk band gap [1–5]. The two materials differ, however, with respect to the topological character of their bulk bands. Whereas pure bismuth is topologically trivial, adding a small amount of Sb into Bi is enough to drive the system into a topological insulator phase [6, 7]. The spin-nondegenerate surface states of the topological insulator $Bi_{(1-x)}Sb_x$ $(0.09 < x < 0.18)$ continuously connect the valence and the conduction band and their existence is derived directly from the fundamental considerations of the parity characteristics of the bulk bands [8]. As more Sb is added into the alloy, the system becomes semimetallic again; it keeps, however, the nontrivial topological order of the bulk bands [7]. Thus, the other extreme case of the $Bi_{(1-x)}Sb_x$ alloy, pure antimony, is a semimetal with bulk characteristic of a strong topological insulator.

The (111) surfaces of the topologically nontrivial materials, including the $Bi_{(1-x)}Sb_x$ alloy and Sb, have been extensively investigated by spin and angle resolved photoemission spectroscopy (ARPES) and scanning tunneling microscopy (STM) [4–7, 9–12]. These studies allowed to determine the spin textures [5, 9, 10], map the surface band dispersion [4–7] and reveal an unconventional electron dynamics [11–13]. At the same time, studies addressing non-(111) surfaces of those materials are almost nonexistent. Only recently, we have shown that Sb(110) exhibits spin-split surface states but, contrary to predictions based on its bulk topology, their dispersion properties are those of a trivial material. This is due to the semimetallic character of the surface, which relaxes the character of the surface state bands imposed by the bulk topology [3]. The spin polarization of these surface bands, however, remains unknown. Since antimony has a weaker spin–orbit coupling than bismuth, it is crucial to show whether a sufficient degree of spin polarization remains in the split surface bands and how it affects its electron scattering properties.

The spin texture of the surface bands can be addressed indirectly by investigating the electron scattering processes [12, 14–17]. The spin–orbit coupling affects the electron scattering probabilities, making them dependent on the overlap of the spin wavefunctions of the final and initial scattering states. In particular, a characteristic feature of spin–orbit coupled systems is the suppression of direct backscattering, because the states with opposite momenta are required to have orthogonal spins by time-reversal symmetry [14, 18]. The modulation in the charge local density of states (LDOS) which arises due to the interference of the electrons scattering at surface impurities is directly accessible with STM and spectroscopy. The scattering vectors q connecting the initial and final states in the reciprocal space can be identified by examining the Fourier transform (FT) of the interference patterns [19]. By demonstrating the lack of backscattering signal, this method allowed to confirm the existence of the spin texture at the surfaces of semimetallic bismuth and antimony [13, 14, 17] as well as topological insulators $Bi_{(1-x)}Sb_x$, Bi_2Se_3 and Bi_2Te_3 [12, 15, 16].

In this paper, we investigate the electron scattering processes on a non-(111) surface of the topologically nontrivial material, Sb(110), in order to gain experimental insight into the spin texture of its surface electronic bands. We observe strong modulation in the LDOS around single adatoms on the surface and correlate the features in the Fourier transformed images to the specific scattering vectors. We identify those scattering events by analyzing the Fermi contour measured by ARPES and the spin polarization of the surface bands predicted by relativistic density functional theory (DFT) calculations. The resulting spin texture is highly anisotropic and strongly varies with the character of the bands, deviating from the conventional picture of a Rashba surface. The experimental STM data do not show any direct backscattering between

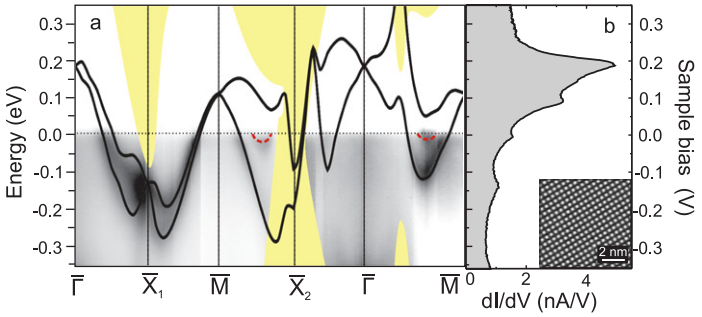

Figure 1. (a) Surface state dispersion of Sb(110) measured by ARPES and calculated by DFT. The ARPES intensity is coded in the gray scale; the continuous lines correspond to the calculated surface states. Yellow shading depicts the projected bulk states. The dashed line highlights the shallow electron pockets revealed by ARPES, but missed in DFT. (b) The $\mathrm{d}I/\mathrm{d}V$ spectrum of a clean Sb(110) surface, showing the LDOS in the bias range of the surface states. The features in the spectrum correspond to the onset of the surface bands. The inset image shows the atomically resolved topography of the clean surface.

the nondegenerate surface bands, confirming their spin-split nature and the spin texture of the Fermi contour.

We have investigated the surface electronic structure of Sb(110) using STM and ARPES. The STM experiments were performed in a custom-made microscope working in an ultrahigh vacuum at 5 K. The ARPES data were taken at the SGM-III beamline of the synchrotron radiation facility ASTRID in Aarhus [20]. The combined energy and angular resolution were better than 10 meV and 0.13°, respectively. The data shown here were all taken using a photon energy of 20 eV. During the photoemission measurements the sample was kept at a temperature of 60 K. The Sb(110) single crystal surface was cleaned *in situ* by repeated sputtering and annealing cycles.

We modeled the electronic and spin structure of Sb(110) using a noncollinear DFT [21] (www.pwscf.org) within the Perdew–Burke–Ernzerhof implementation [22] of the generalized gradient approximation. We considered a repeated slab system consisting of 54 layers relaxed up to forces $<10^{-4}$ Ryd au^{-1} and used fully relativistic norm-conserving pseudopotentials as described in [21] with the energy cutoff corresponding to $E_c = 60$ Ryd. In order to calculate the projection of the bulk band structure onto the (110) surface, we have also used the tight-binding scheme of Liu and Allen [23].

The Sb(110) surface shows several spin–orbit split surface states within the projected bulk band gap. In figures 1 and 2, we present the electronic structure of Sb(110) as measured by ARPES and calculated by DFT. The dispersion of the surface bands and their topological character were discussed in detail in [3]. Here, we summarize the most important properties of this surface, which directly affect the electron scattering processes, i.e. the dispersion of the surface bands in the vicinity of the Fermi level and their spin texture. The electronic structure of Sb(110) along certain high-symmetry directions is shown in figure 1(a) and the experimentally determined Fermi contour is presented in figure 2(c) (grayscale background). For clarity, the lines have been superimposed on the data in figure 2(c), showing schematically the shape of the contour. The most important spectroscopic features that we identify in both calculations and

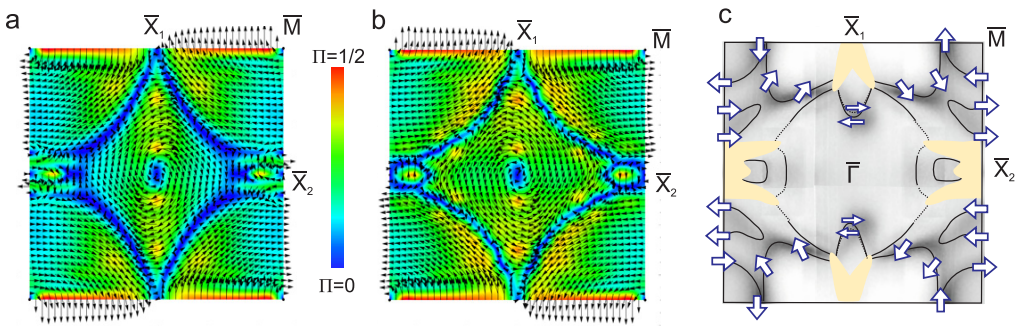

Figure 2. Calculated spin texture within the first surface Brillouin zone, for the lower (a) and upper (b) subbands. The color code represents the degree of the spin polarization Π (see text for details), arrows show the direction of the spin in the surface plane. (c) Fermi contour of Sb(110) measured by ARPES. The continuous lines are a schematic representation of the ARPES data; the dotted line represents parts of the contour with vanishing ARPES intensity. The arrows schematically show the spin polarization of the contour, as deduced from the plots in (a) and (b).

the experimental data are: (i) the hole pocket around the $\bar{M}$ point, giving rise to circular contour in figure 2(c), (ii) a pocket around $\bar{X}_1$, identified in the Fermi contour as a 'butterfly'-shaped feature; and (iii) an extended hole pocket around $\bar{\Gamma}$, observed as a weak feature in ARPES data. In addition, ARPES reveals a very shallow electron pocket (dotted lines in figure 1(a) in the $\bar{X}_2\bar{M}$ and $\bar{\Gamma}\bar{M}$ directions), which is not well reproduced by the calculations. This pocket is particularly important for understanding the electron scattering dynamics in the vicinity of the Fermi level, since it contributes strongly to the density of states in this energy window [14]. In fact, the experimentally measured $\mathrm{d}I/\mathrm{d}V$ spectrum (figure 1(b)), which reflects the LDOS of a clean Sb(110) surface, shows a peak in the vicinity of the Fermi level, marking the onset of the electron pocket. Several other sharp features in the $\mathrm{d}I/\mathrm{d}V$ spectrum correspond to the onset (negative bias) and the top (positive bias) of the surface bands. Due to the relatively weak spin–orbit coupling in Sb, the splitting of the bands is rather small so that in certain parts of the Brillouin zone the two spin partners are close to being degenerate. Accordingly, some of the features of the Fermi contour in figure 2(c), the high-intensity feature along the $\bar{\Gamma}\bar{X}_1$ direction and crossing along the $\bar{X}_1\bar{M}$ direction, are double crossings and the two states with opposite spin become almost degenerate.

To determine the spin of the Fermi contour we calculated the spin texture of the upper and lower subbands within the first Brillouin zone, as shown in figures 2(a) and (b), respectively. The degree of certainty about the electron spin, $\Pi \equiv \sqrt{\sum_i \langle S_i \rangle^2}$, is represented by the color scale in the background ($\Pi \in [0, 1/2]$). The direction of the spin in the surface plane is depicted by arrows. The polarization out of plane becomes important only for the lower subband, close to the $\bar{X}_2$ point. Across the rest of the Brillouin zone, the expectation value of the polarization out of plane remains very small. The spin texture of any constant energy contour can now be defined by considering separately the spin polarization for the lower and upper subbands. In figure 2(c) the spin polarization deduced from the plots in (a) and (b) is superimposed on the Fermi contour of Sb(110). We find that the spin direction is almost constant as we move along one side of the butterfly-shaped pocket and rotates along the $\bar{M}$ pockets. The features along

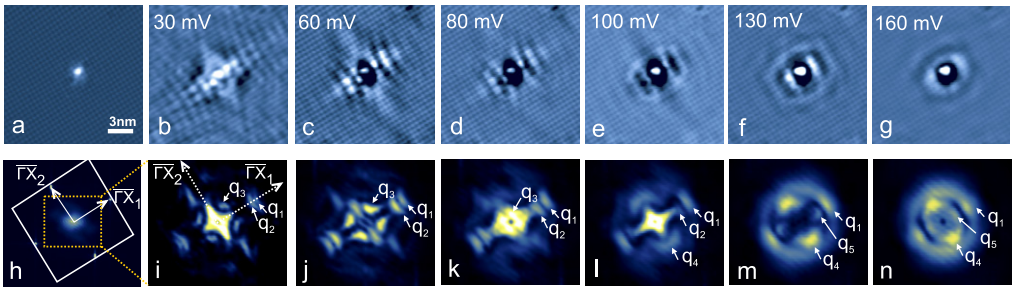

Figure 3. STM imaging of the interference patterns formed around a single impurity atom on Sb(110). The adatoms (presumably Sb) have been obtained by control tip indentation in the substrate. (a) Constant current topography image of the impurity ($I = 0.5$ nA, $V = 60$ mV). (b)–(g) Energy resolved $\mathrm{d}I/\mathrm{d}V$ images showing electron interference patterns, at bias voltages 30, 60, 80, 100, 130 and 160 mV, respectively. A corresponding FFT image is shown below each real space image: (h)–(n). The full FFT of the topography image (h) shows the main crystal directions and bright points corresponding to the atomic corrugation. Images (i)–(n) have been cut out of the full FFT (dotted square in (h)) for a more detailed view of the scattering vectors. The origin of features q_1–q_5 are described in the text.

$\bar{\Gamma}\bar{X}_1$ and $\bar{X}_1\bar{M}$ correspond to almost double crossings and, consequently, have contributions from both spin-split bands, and thus, two opposite spins.

The spin texture of the constant energy contours will affect the scattering of the electrons by the surface impurities. In particular, the systems with spin–orbit split surface states are characterized by the absence of direct backscattering, imposed by the time-reversal symmetry [18]. In order to experimentally verify the spin texture of Sb(110) and identify the allowed scattering vectors, we analyzed the charge interference patterns formed by electrons scattering on a single adatom (figure 3). In the bias range between −80 and 240 meV, we observe pronounced modulation in the LDOS signal. A series of $\mathrm{d}I/\mathrm{d}V$ spectroscopic images in figures 3(b)–(g) shows the evolution of patterns for several chosen bias voltages. The fast Fourier transform (FFT) of the images ((i)–(n)) shows high intensity features (labeled in figures 3–5 as q_i, with $i = 1, \ldots, 5$) revealing a set of allowed scattering vectors $\vec{q}$.

Close to the Fermi level ((i) and (j)) the most distinctive features of the FFT[9] are two double arc-shaped features along the $\bar{\Gamma}\bar{X}_1$ direction (labeled q_1 and q_2) and four spots lying symmetrically around the center (labeled q_3). The features disperse with increasing the sample bias as shown in more detail in figures 4(a)–(c). Each graph represents a set of the line scans through the FFT images taken at different sample bias in a certain high-symmetry direction ($\bar{\Gamma}\bar{X}_1$, $\bar{\Gamma}\bar{M}$ and $\bar{\Gamma}\bar{X}_2$, respectively). The k-vectors pointing to features q_1 and q_2 get smaller until at around 100 meV the feature q_2 vanishes from the FFT and the q_1 transforms into a circular shape. The four features q_3 move to the center of the FFT and disappear also at around 100 meV. At the same bias range two more scattering events appear: the features q_4 in the direction $\bar{\Gamma}\bar{X}_2$ and q_5 in the direction $\bar{\Gamma}\bar{X}_1$.

[9] Additional features as those close to the line connecting Γ and X_2 are not studied here due to the absence of clear dispersion patterns, which makes their association with a certain scattering event more speculative.

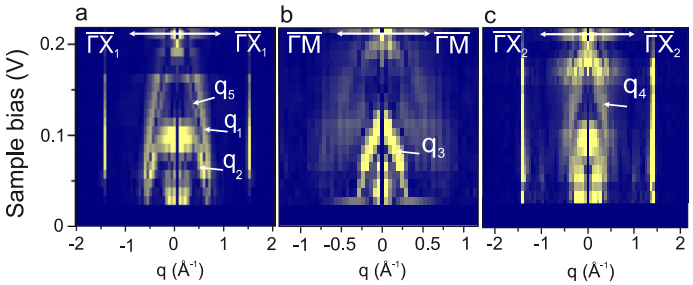

Figure 4. Dispersion of the scattering vectors in the directions $\bar{\Gamma}\bar{X}_1$ (a), $\bar{\Gamma}\bar{M}$ (b) and $\bar{\Gamma}\bar{X}_2$ (c). The nondispersive points correspond to the atomic corrugation spots in the FFT. The labeling of high intensity features is the same as in figure 3.

In order to establish the origin of the features observed in FFT, we consider the shape and spin texture of the constant energy contour. In the simple picture, the scattering probability $P(\vec{q}, eV)$ at energy eV, between the $\vec{k}$-states separated by the scattering vector $\vec{q}$, is determined by the electron density of states ρ of the final and the initial state, weighted by the overlap of the spinor wavefunctions φ_S [12]:

$$P(\vec{q}, eV) = \int \rho(\vec{k}, eV)\rho(\vec{k}+\vec{q}, eV)\langle\varphi_S(\vec{k})|\varphi_S(\vec{k}+\vec{q})\rangle \, \mathrm{d}^2\vec{k}. \tag{1}$$

Thus, the spin-dependent part of the scattering amplitude will be maximal if the initial and final spins are parallel and zero if the two spins are antiparallel.

If the spin contribution to the scattering amplitudes is neglected, the map of the scattering vectors allowed by the Fermi contour can be evaluated directly from the photoemission data by calculating the convolution of the ARPES spectra. The autocorrelation image (AC-ARPES) can be derived from the ARPES intensities $I(\vec{k}, eV)$ as [24, 25]

$$\text{AC-ARPES}(\vec{q}, eV) = \int I(\vec{k}, eV) I(\vec{k}+\vec{q}, eV) \, \mathrm{d}^2\vec{k}. \tag{2}$$

The AC-ARPES defined in this way reproduces the features of the joint density of states (JDOS), which in turn maps out the LDOS contribution to the scattering probabilities. While the quantitative comparison between AC-ARPES and JDOS is not straightforward, since the ARPES intensities I are related to the electron spectral function through an energy and k-dependent matrix element, the autocorrelation image stills allows for a qualitative analysis of the scattering vectors [24, 25]. For spin degenerate Fermi contour, the AC-ARPES can be directly compared with the FFT of the interference patterns resolved by STM at low bias [25].

We have calculated the AC-ARPES map for Sb(110) (figure 5(a)), neglecting its spin texture, and compared it with the FT-STM map measured close to the Fermi level (figure 5(d)). We find that certain parts of the AC-ARPES are suppressed in the STM data. In fact, many of the features present in AC-ARPES but absent in the FFT map can be identified as direct backscattering events, which are expected to be prohibited by the spin texture of Sb(110). Thus, to describe the experimental STM data more accurately, we introduce into the cross-correlation integral (equation (2)) an additional term: $\frac{1}{2}/1+\cos[\angle(\vec{k}, \vec{k}+\vec{q})]$. While this basic term does not account for the anisotropic spin texture of Sb(110), it suppresses the backscattering in a simple way. The result (figure 5(b)) reproduces the FFT map to a greater degree. Large

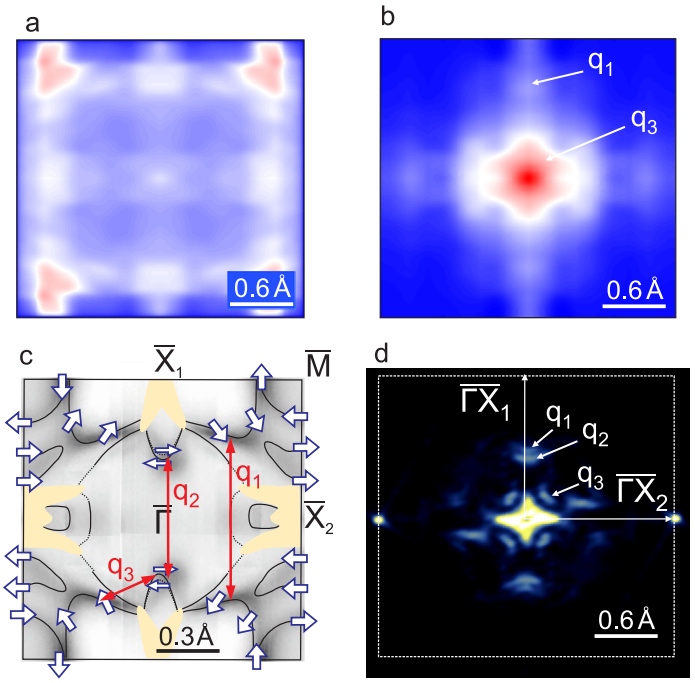

Figure 5. (a) The autocorrelation of the ARPES data of the Fermi contour of Sb(110), neglecting its spin texture. (b) The autocorrelation signal as in (a), but with suppressed backscattering (see the text for details). (c) The Fermi contour of Sb(110) with the identified scattering vectors. (d) FFT measured at bias close to the Fermi level (30 mV).

parts of the original AC-ARPES map in figure 5(b) are now diminished and the remaining features correspond relatively well to the main spots of the FFT. We can thus conclude that the backscattering is indeed absent on the Sb(110) surface, confirming the spin-split character of its surface bands.

We can now associate the spots resolved in the FT-STM map (figure 5(d)) with the specific scattering vectors. First, we identify the feature q_1 as interband scattering between the edges of the 'butterfly wings' in the $\bar{\Gamma}\bar{X}_1$ direction (figure 5(c)). This feature of the Fermi contour corresponds to a very shallow and extended electron pocket and is thus expected to have a high DOS and contribute strongly to the scattering at this energy range. With increasing bias, q_1 disperses very steeply (see figure 4(a)), reflecting the dispersion of the left band which forms the electron pocket in the $\bar{\Gamma}\bar{M}$ direction. In principle, the scattering between the 'butterfly wings' should also give rise to features in FFT in the $\bar{\Gamma}\bar{X}_2$ direction. They are indeed resolved in the AC-ARPES images (figure 5(a)) but we observe them only as faint spots in the FT-STM image, possibly due to partial suppression by the overlap of the spinor wavefunctions. Next, we assign the feature q_2 to the backscattering between the $\bar{\Gamma}\bar{X}_1$-crossing points. At first glance, such a scattering event seems to violate the time-reversal symmetry. However, at this point of the Fermi contour the two spin-split bands are close to being degenerate. Therefore both spin partners are present, allowing the backscattering process, in a similar way as it happens on an Au(111) surface [18]. Since backscattering is a preferred scattering process on metal surfaces, this feature has a rather high intensity in the FFT [18]. The AC-ARPES map in figure 4(b) does

not reproduce it however, as the $\frac{1}{2}/1+\cos[\angle(\vec{k},\vec{k}+\vec{q})]$ term included in the integral excludes all the backscattering processes. This assignment of q_2 is further confirmed by the bias evolution of this feature (figure 4(a)). As the energy increases, the bands that cross the Fermi level along the $\bar{\Gamma}\bar{X}_1$ direction disperse toward the $\bar{\Gamma}$ point. Thus, the feature q_2 moves toward the center of the FT-STM image (figure 4(a)), until the top of the band is reached, and it disappears from the FFT. This point at ∼100 meV is not accurately reproduced by the band structure calculations in figure 1(a) (∼190 meV), which we attribute to the inability of DFT to reproduce all fine structure details in the meV range. The spots marked as q_3 result from the forward scattering between the edges of the butterfly wing (the electron pocket) and the $\bar{\Gamma}\bar{X}_1$-crossing point. The analysis of the band's dispersion also shows that these features should move toward the center of the FFT image (figure 4(c)).

The identification of the scattering events far above the Fermi level (q_4 and q_5) is not as clear, because of the uncertainties in the calculated dispersion and the absence of photoemission data. We can tentatively explain their origin by the appearance of the new high DOS feature (peak at 100 meV in figure 1(b)), when the sample bias reaches the top of the bands near the $\bar{M}$ and $\bar{\Gamma}$ points.

It is interesting to compare these results with the previous study of electron scattering on Bi(110), another extreme case of the BiSb alloy. In Bi(110) the pronounced spin splitting of the surface bands leads to a clear manifestation of the spin-dependent scattering process. In fact, only spin conserving scattering events are observed in the Fourier transformed $\mathrm{d}I/\mathrm{d}V$ maps on Bi(110) [14, 17].

Antimony has a smaller spin–orbit coupling and the spin split of the bands is generally smaller [3]. Although the bands maintain a certain spin texture (as evidenced in figure 2), the role of the spin in the formation of interference patterns is experimentally less evident, and certain backscattering events could be identified. These are caused because, at certain points of the Fermi surface with high DOS, the two sub-bands are so close in k-space that the scattering between them will resemble the backscattering events in the interference patterns, in a similar way as that described in [18].

In summary, we have predicted theoretically and confirmed experimentally the unconventional spin texture of the Sb(110) surface. In spite of a smaller spin–orbit coupling, the spin polarization of the surface bands still dominates the electron dynamics of this surface. The LDOS interference patterns formed around single impurities reveal the dominance of nondirect backscattering events as in the related compound Bi(110). Identification of the scattering events was done combining ARPES measurements at E_F with the state's dispersion above E_F, measured from energy-dependent differential conductance maps and interpreted on the basis of DFT calculations of the spin texture and dispersion of the surface state bands. The smaller spin–orbit interaction of Sb(110) is reflected in a smaller band splitting that, in some cases, gives rise to interband scattering with wavevectors close to the pure backscattering case.

Acknowledgments

The authors gratefully acknowledge support from the Deutsche Forschungsgemeinschaft (STR 1151/1-1), the Spanish Ministry of Science and Innovation (FIS2010-19609-C02-00) and the Danish Council for Independent Research—Natural Sciences.

References

[1] Agergaard A, Søndergaard Ch, Li H, Nielsen M B, Hoffmann S V, Li Z and Hofmann Ph 2001 *New J. Phys.* **3** 15

[2] Hofmann Ph 2006 *Prog. Surf. Sci.* **81** 191

[3] Bianchi M, Guan D, Strozecka A, Voetmann C H, Bao S, Pascual J I, Eiguren A and Hofmann Ph 2012 *Phys. Rev.* B **85** 155431

[4] Sugawara K, Sato T, Souma S, Takahashi T, Arai M and Sasaki T 2006 *Phys. Rev. Lett.* **96** 046411

[5] Kadono T, Miyamoto K, Nishimura R, Kanomaru K, Qiao S, Shimada K, Namatame H, Kimura A and Taniguchi M 2008 *Appl. Phys. Lett.* **93** 252107

[6] Hsieh D, Qian D, Wray L, Xia Y, Hor Y S, Cava R J and Hasan M Z 2008 *Nature* **452** 970

[7] Guo H *et al* 2011 *Phys. Rev.* B **83** 201104

[8] Teo J C Y, Liang Fu and Kane C L 2008 *Phys. Rev.* B **78** 045426

[9] Hsieh D *et al* 2009 *Science* **323** 919

[10] Hsieh D *et al* 2010 *New J. Phys.* **12** 125001

[11] Park S R *et al* 2011 *New J. Phys.* **13** 013008

[12] Roushan P, Seo J, Parker C V, Hor Y S, Hsieh D, Qian D, Richardella A, Hasan M Z, Cava R J and Yazdani A 2009 *Nature* **460** 1106

[13] Gomes K K, Ko W, Mar W, Chen Y, Shen Z X and Manoharan H C 2009 arXiv:0909.0921

[14] Pascual J *et al* 2004 *Phys. Rev. Lett.* **93** 196802

[15] Alpichshev Z, Analytis J G, Chu J H, Fisher I R, Chen Y L, Shen Z X, Fang A and Kapitulnik A 2010 *Phys. Rev. Lett.* **104** 016401

[16] Zhang T *et al* 2009 *Phys. Rev. Lett.* **103** 016401

[17] Strozecka A, Eiguren A and Pascual J I 2011 *Phys. Rev. Lett.* **107** 186805

[18] Petersen L and Hedegard P 2000 *Surf. Sci.* **459** 49

[19] Petersen L, Sprunger P T, Hofmann Ph, Lagsgaard E, Briner B G, Doering M, Rust H P, Bradshaw A M, Besenbacher F and Plummer E W 1998 *Phys. Rev.* B **57** 6858

[20] Hoffmann S V, Sondergaard C, Schultz C, Li Z and Hofmann Ph 2004 *Nucl. Instrum. Methods Phys. Res.* A **523** 441

[21] Dal Corso A and Mosca Conte A 2005 *Phys. Rev.* B **71** 115106

[22] Perdew J P, Burke K and Ernzerhof M 1996 *Phys. Rev. Lett.* **77** 3865

[23] Liu Y and Allen R E 1995 *Phys. Rev.* B **52** 1566

[24] Markiewicz R S 2004 *Phys. Rev.* B **69** 214517

[25] McElroy K, Gweon G H, Zhou S, Graf J, Uchida S, Eisaki H, Takagi H, Sasagawa T, Lee D H and Lanzara A 2006 *Phys. Rev. Lett.* **96** 067005